Geoscientific
Model Development

Incorporation of volcanic SO₂ emissions in the Hemispheric CMAQ (H-CMAQ) version 5.2 modeling system and assessing their impacts on sulfate aerosol over the Northern Hemisphere

Syuichi Itahashi[1], **Rohit Mathur**[2], **Christian Hogrefe**[2], **Sergey L. Napelenok**[2], and **Yang Zhang**[3]

[1]Sustainable System Research Laboratory (SSRL), Central Research Institute of Electric Power Industry (CRIEPI),
1646 Abiko, Abiko, Chiba 270–1194, Japan
[2]Center for Environmental Measurement and Modeling, Office of Research and Development,
US Environmental Protection Agency, Research Triangle Park, NC 27711, USA
[3]Department of Civil and Environmental Engineering, Northeastern University, Boston, MA 02115, USA

Correspondence: Syuichi Itahashi (isyuichi@criepi.denken.or.jp)

Abstract. The state-of-the-science Community Multiscale Air Quality (CMAQ) Modeling System has recently been extended for hemispheric-scale modeling applications (referred to as H-CMAQ). In this study, satellite-constrained estimation of the degassing SO₂ emissions from 50 volcanoes over the Northern Hemisphere is incorporated into H-CMAQ, and their impact on tropospheric sulfate aerosol (SO_4^{2-}) levels is assessed for 2010. The volcanic degassing improves predictions of observations from the Acid Deposition Monitoring Network in East Asia (EANET), the United States Clean Air Status and Trends Network (CASTNET), and the United States Integrated Monitoring of Protected Visual Environments (IMPROVE). Over Asia, the increased SO_4^{2-} concentrations were seen to correspond to the locations of volcanoes, especially over Japan and Indonesia. Over the USA, the largest impacts that occurred over the central Pacific were caused by including the Hawaiian Kilauea volcano, while the impacts on the continental USA were limited to the western portion during summertime. The emissions of the Soufrière Hills volcano located on the island of Montserrat in the Caribbean Sea affected the southeastern USA during the winter season. The analysis at specific sites in Hawaii and Florida also confirmed improvements in regional performance for modeled SO_4^{2-} by including volcanoes SO₂ emissions. At the edge of the western USA, monthly averaged SO_4^{2-} enhancements greater than $0.1\,\mu g\,m^{-3}$ were noted within the boundary layer (defined as surface to 750 hPa) during June–September. Investigating the change on SO_4^{2-} concentration throughout the free troposphere revealed that although the considered volcanic SO₂ emissions occurred at or below the middle of free troposphere (500 hPa), compared to the simulation without the volcanic source, SO_4^{2-} enhancements of more than 10 % were detected up to the top of the free troposphere (250 hPa). Our model simulations and comparisons with measurements across the Northern Hemisphere indicate that the degassing volcanic SO₂ emissions are an important source and should be considered in air quality model simulations assessing background SO_4^{2-} levels and their source attribution.

1 Introduction

Airborne sulfate (SO_4^{2-}) is one of the major components of tropospheric particulate matter worldwide (Zhang et al., 2007) and plays important roles in modulating the earth–atmosphere energy budget, atmospheric circulation, cloud properties, and precipitation (Seinfeld and Pandis, 2016). SO_4^{2-} is produced via the aqueous- and gas-phase oxidation of sulfur dioxide (SO_2), and these processes are well understood (Seinfeld and Pandis, 2016). The dominant sources of SO₂ emissions are attributed to anthropogenic activity (Warneck and Williams, 2012). The global anthropogenic SO₂ emissions peaked in the early 1970s with around $130\,Tg\,yr^{-1}$

and then decreased; however, this emission trend has contrasting characteristics over the USA and Asia (e.g., Smith et al., 2011; Xing et al., 2015a). Anthropogenic SO$_2$ emissions from the USA showed a peak in the early 1970s with 30 Tg yr^{-1} and subsequently decreased (Smith et al., 2011). Publicly available observational records have begun from the late 1980s over the USA, and it has been confirmed that SO$_4^{2-}$ concentration in the USA decreased during the early 1990s through 2010 in response to these reductions in SO$_2$ emissions as evidenced in analyses of observational aerosol composition (e.g., Hand et al., 2012; Gan et al., 2015). On the other hand, anthropogenic SO$_2$ emissions across Asia, especially China, have shown a continuous increase since 1970 (Smith et al., 2011) up to 2006 and then decreased (Li et al., 2017) in response to control measures. These multi-decadal changes in SO$_2$ emissions have resulted in not only contrasting changes in tropospheric SO$_4^{2-}$ levels but also in aerosol radiative effects (e.g., Wild et al., 2009; Xing et al., 2015b), their feedback on atmospheric dynamics and air quality (e.g., Xing et al., 2016), and acid deposition (e.g., Zhang et al., 2018; Mathur et al., 2020).

As SO$_2$ emission control is reducing regional airborne SO$_4^{2-}$, quantifying the relative contribution of long-range transported SO$_4^{2-}$ and the portion attributable to natural sources is becoming increasingly important. For instance, regional haze assessments require quantification of visibility impairment that are associated with anthropogenic enhancements over natural visibility levels, which in turn necessitates accurate quantification of the contribution of natural sources. Next to the anthropogenic emissions, volcanic emissions have an important contribution to SO$_2$ emissions (Warneck and Williams, 2012). A time-averaged inventory of volcanic emissions was estimated as 13 Tg SO$_2$ yr^{-1} during the early 1970s to 1997, and these volcanoes are mostly located in the Pacific Rim region (Andres and Kasgnoc, 1998). Volcanic emission fluxes can be measured in several ways such as a correlation spectrometer (COSPEC), but observable volcanic eruptions are limited in time and location. Satellite observations are now proving to be a useful approach to monitor the volcanic emissions and have provided a global volcanic SO$_2$ emission inventory since 1978 (Carn et al., 2016). Accurate representation of volcanic emissions requires quantification of emissions emitted from both persistent degassing and sporadic eruptions. Recently, a decadal-scale global volcanic SO$_2$ emissions inventory for the 2005–2015 period, constrained by the Ozone Monitoring Instrument (OMI), has been established (Carn et al., 2017). The enhanced methodology with greater sensitivity allows the detection of emissions as low as approximately 6 Gg SO$_2$ yr^{-1} for low-altitude volcanoes and covers a total of 91 persistently degassing volcanic SO$_2$ sources. The volcanic SO$_2$ emissions from degassing are relatively stable at 23.0 ± 2.3 Tg SO$_2$ yr^{-1} during 2005–2015, and the highest amount was approximately 26 Tg SO$_2$ yr^{-1} in 2010. In terms of the volcanic activity,

sporadic eruptions inject into the atmosphere comparatively large amounts of SO$_2$ emissions. For example, one of the largest eruptions in the 1990s was that of Mt. Pinatubo in June 1991, which was estimated to have injected 18 Tg of SO$_2$ emissions into the atmosphere (Smithsonian Institution, 2020). The injection heights of that eruption reached to more than 30 km and caused the largest perturbations ever observed in the chemical state of the stratosphere and the earth–atmosphere radiation budget (McCormick, et al., 1995). However, such eruptive emissions are temporary. According to the comparison between the degassing and eruptive emissions, Carn et al. (2017) estimated that during 2005–2015, volcanic activity contributed about 23 Tg yr^{-1} of SO$_2$ due from degassing while eruptive SO$_2$ emissions ranged from 0.2 to 10 Tg yr^{-1} of SO$_2$. Therefore, understanding the behavior of the degassing SO$_2$ emissions and its contributions to airborne SO$_4^{2-}$ levels is important. For example, it was reported that although volcanic SO$_2$ emissions contributed 15 % to the total sulfur emissions, it attributed 27 % of the tropospheric sulfur budget (Lamotte et al., 2021).

Numerical modeling is a useful tool to characterize source–receptor relationships. Regional modeling studies have already indicated that volcanic SO$_2$ emissions are one of the main sources of SO$_4^{2-}$ over Japan (Itahashi et al., 2017a, b, 2019; Itahashi, 2018). SO$_2$ emissions from volcanoes in the Pacific Rim region not only regulate tropospheric SO$_4^{2-}$ levels in surrounding countries but through long-range transport can also potentially impact SO$_4^{2-}$ distributions over the Pacific and background levels in the western USA. Liu et al. (2008) for instance suggest that west to east across the North Pacific, sulfate originating from East Asia sources contributed approximately 80 %–20 % of sulfate at the surface, but at least 50 % at 500 hPa. Taking into consideration that volcanoes are mainly over the Pacific Rim area and the seasonally prevalent cross-Pacific transport patterns, volcanic SO$_2$ emissions could also affect SO$_4^{2-}$ concentrations over North America. While previous studies have attempted to quantify global tropospheric SO$_4^{2-}$ budgets (e.g., Chin et al., 1996; Chin and Jacob, 1996), the assessments are representative of conditions in the late 1980s to early 1990s. Since anthropogenic SO$_2$ emissions have changed significantly over the past several decades, and since recent studies provide improved constraints of volcanic SO$_2$ emissions, the work summarized in this article attempts to assess the contributions of volcanic SO$_2$ emissions on tropospheric SO$_4^{2-}$ distributions across the Northern Hemisphere and North America. We specifically focus on assessing the impacts of the persistent degassing volcanic SO$_2$ emissions.

This article is organized as follows. In Sect. 2, the modeling system and simulation setup are described along with the ground-based observations used to evaluate the model performance. In Sect. 3, the model results and comparisons with observations are presented, and the impact of including volcanic SO$_2$ emissions is discussed. Finally, Sect. 4 sum-

marizes the key results and limitations of this work and discusses future perspectives.

2 Methodology

2.1 Hemispheric CMAQ modeling system and its setup

The Community Multiscale Air Quality (CMAQ) modeling system version 5.2 extended for hemispheric applications (H-CMAQ) (Sarwar et al., 2015; Xing et al., 2015a; Mathur et al., 2017; Itahashi et al., 2020a, b) is used to incorporate and assess the impacts from volcanic SO$_2$ emissions. H-CMAQ is configured to cover the entire Northern Hemisphere, utilizing a polar stereographic horizontal discretization of 187×187 grid points with a grid spacing of 108 km and a terrain-following vertical coordinate system with 44 layers of variable thickness from the surface up to 50 hPa. The emission datasets for the base case H-CMAQ simulation are based on the Hemispheric Transport of Air Pollution version 2 (HTAP2) experiments. The details were described in previous studies (Janssens-Maenhout et al., 2015; Pouliot et al., 2015; Galmarini et al., 2017; Hogrefe et al., 2018). Over the modeling domain, a total of 105.8 Tg yr^{-1} of SO$_2$ emissions is emitted. The spatial distribution of SO$_2$ emissions is shown in Fig. 1a with high SO$_2$ emissions from fossil fuel combustion activities in North America, Europe including western Russia, and Asia, with relatively higher amounts across regions in China and India as described in Janssens-Maenhout et al. (2015). The CMAQ configuration employed the CB05 gas-phase chemical mechanism and the aero6 module with nonvolatile primary organic aerosol (POA) (Appel et al., 2017; Simon and Bhave, 2012). CMAQ treats one gas-phase oxidation and five aqueous-phase oxidations for converting S(IV) (i.e., sulfur compounds with oxidation state 4) into S(VI) (i.e., sulfur compounds with oxidation state 6). The gas-phase oxidation involves reaction with hydroxyl (OH) radical, and five aqueous-phase reactions involve oxidation by hydrogen peroxide (H$_2$O$_2$), ozone (O$_3$), oxygen (O$_2$) via Fe and Mn catalysis, methyl hydrogen peroxide (MHP), and peroxyacetic acid (PAA). The meteorological fields to drive H-CMAQ are derived from simulations with the Weather Research and Forecasting (WRF) model version 3.6.1. The WRF model is configured to use the rapid radiative transfer model for global climate models (RRTMG) radiation scheme for both longwave and shortwave (Iacono et al., 2008), Morrison double-moment scheme (Morrison et al., 2009) and the Kain–Fritsch (KF) cumulus parameterization (Kain, 2004) for microphysics and cumulus parameterization, and Mellor–Yamada–Janjic scheme for planetary boundary layer (Janjic et al., 1994). In this study, the entire year of 2010 was simulated to analyze the volcanic emission impacts over the Northern Hemisphere, as the SO$_2$ emissions from degassing during the 2005–2015 period were highest in 2010. Also note that emission estimates presented in Carn

et al. (2017) suggest that degassing dominate over eruptive SO$_2$ emissions during the same time period. The WRF simulations used nudging for wind, temperature, and water vapor fields towards NCEP final analysis (FNL) of 1° spatial and 6 h temporal resolution (NCEP, 2020) over the entire vertical model extent. WRF simulation started from 1 January 2009 to set one year spinup time prior to the analysis period the year of 2010 as recommended by Mathur et al. (2017). The CMAQ simulation was initialized on 1 December 2009 with three-dimensional chemical fields from prior model simulations for 2010 by Hogrefe et al. (2018).

Earlier development and applications with the H-CMAQ modeling system have not considered volcanic SO$_2$ emissions. In this study, degassing volcanic SO$_2$ emissions as annual amount estimated by Carn et al. (2017) are incorporated into H-CMAQ. The estimated emission of SO$_2$ from the 50 volcanoes within our Northern Hemisphere modeling domain (Fig. 1b) is 12.7 Tg yr^{-1}. Considering the characteristics of degassing process from volcanoes and the lack of any other information to accurately specify its temporal variations, we use a constant SO$_2$ emission rate in H-CMAQ based on the annual SO$_2$ emission estimates by Carn et al. (2017). Table 1 provides detailed information on these 50 volcanoes including name, location (longitude and latitude), altitude (as above sea level (a.s.l.)), and SO$_2$ emission rate. Kilauea located in Hawaii is estimated to have the highest amount of degassing SO$_2$ emissions. Taking into account the characteristics of the degassing process, volcanic degassing SO$_2$ emissions were allocated into the model vertical layer corresponding to the volcano's altitude. This approach was also taken in another global model analysis (Chin et al., 1996; Ge et al., 2016). Even though in principle volcanic degassing emissions could be assigned to the first model layer because CMAQ uses a terrain-following vertical coordinate system, the 108 km grid spacing used in CMAQ does not allow the model to adequately resolve localized terrain peaks such as volcanoes, and assigning their emissions to the first model layer would not account for the fact that in reality these emissions typically occur above the mixed layer. Therefore, the vertical layer to which volcanic degassing emissions were assigned was determined by first calculating the difference between the altitude of a given volcano (Table 1) and the CMAQ terrain height for the cell in which it is located and then determining the vertical CMAQ layer corresponding to this difference. A schematic of the resultant assigned vertical layer is illustrated in Fig. 2. Most of volcanoes are located between altitudes of 500–5000 m a.s.l. (Table 1), and these correspond to layers 11–26 in the current model configuration.

2.2 Ground-based observations

As seen from Fig. 1b, the majority of the degassing volcanoes are located in the Pacific Rim region and their impacts on SO$_4^{2-}$ levels in Japan have previously been studied

Table 1. Information of volcanoes incorporated in this study.

| No.	Name	Country	Longitude [°]	Latitude [°]	Altitude [m a.s.l]	Emission [Gg yr^{-1}]
1	Kilauea	USA	−155.29	19.42	1222.0	2739.0
2	Mutnovsky + Gorely	Russia	158.20	52.45	2322.0	960.4
3	Dukono	Indonesia	127.88	1.68	1170.0	848.9
4	Turrialba + Poás	Costa Rica	−83.77	10.03	3340.0	788.5
5	Soufriére Hills	Montserrat (UK)	−62.18	16.72	870.0	667.1
6	Kliuchevskoi + Bezymianny	Russia	160.64	56.06	4835.0	631.2
7	Nevado del Huila	Colombia	−76.03	2.93	5364.0	617.6
8	Etna	Italy	15.00	37.73	2711.0	533.3
9	Sakurajima	Japan	130.65	31.59	1117.0	443.5
10	Popocatépetl	Mexico	−98.62	19.02	5100.0	372.1
11	Suwanosejima	Japan	129.71	29.64	796.0	349.3
12	Shiveluch	Russia	161.34	56.64	3283.0	334.7
13	Mayon	Philippines	123.69	13.26	2462.0	293.7
14	Karymsky	Russia	159.45	54.05	1536.0	280.2
15	Miyakejima	Japan	139.53	34.09	775.0	276.7
16	Sarychev	Russia	153.21	48.08	1200.0	267.3
17	Pagan	Northern Mariana Islands	145.79	18.14	570.0	244.5
18	Masaya	Nicaragua	−86.16	11.98	635.0	221.3
19	Avachinsky	Russia	158.83	53.25	2741.0	218.1
20	San Cristóbal + Telica	Nicaragua	−87.00	12.70	1745.0	206.0
21	Aso	Japan	131.10	32.88	1592.0	149.2
22	Satsuma-Iojima	Japan	130.31	30.79	704.0	131.0
23	Shishaldin	USA	−163.97	54.76	2857.0	87.4
24	Chikurachki + Ebeko	Russia	155.46	50.33	1816.0	85.0
25	Asama	Japan	138.52	36.41	2568.0	80.3
26	Fuego + Pacaya	Guatemala	−90.88	14.47	3763.0	77.0
27	Redoubt	USA	−152.75	60.49	3108.0	75.7
28	Bulusan	Philippines	124.05	12.77	1500.0	71.5
29	Stromboli	Italy	15.21	38.79	870.0	61.6
30	Karangetang	Indonesia	125.40	2.78	1780.0	53.3
31	Santa Maria	Guatemala	−91.55	14.76	3772.0	51.5
32	Sinabung	Indonesia	98.39	3.17	2460.0	46.4
33	Tokachi	Japan	142.69	43.42	2077.0	45.0
34	Lokon-Empung	Indonesia	124.79	1.36	1580.0	44.4
35	Ketoi	Russia	152.48	47.34	870.0	34.3
36	Kudriavy	Russia	148.84	45.39	1125.0	34.1
37	Augustine	USA	−153.45	59.35	1252.0	32.8
38	Gareloi	USA	−178.79	51.79	1573.0	30.9
39	Spurr	USA	−152.25	61.30	3374.0	28.2
40	Veniaminof	USA	−159.38	56.17	2507.0	27.7
41	Anatahan	Northern Mariana Islands	145.67	16.35	320.0	26.8
42	Barren Island	India	93.86	12.28	230.0	24.6
43	Galeras	Colombia	−77.39	1.20	4276.0	22.8
44	Santa Ana	El Salvador	−89.63	13.85	2381.0	18.2
45	Alu-Dalafilla + Erta Ale	Ethiopia	40.67	13.60	613.0	16.7
46	Cleveland	USA	−169.77	52.83	1170.0	16.3
47	Jebel at Tair	Yemen	41.83	15.55	244.0	11.2
48	Kizimen	Russia	160.36	55.12	2376.0	10.1
49	Kanlaon	Philippines	123.13	10.41	2435.0	10.0
50	Nevado del Ruiz	Colombia	−75.32	4.90	5321.0	1.2
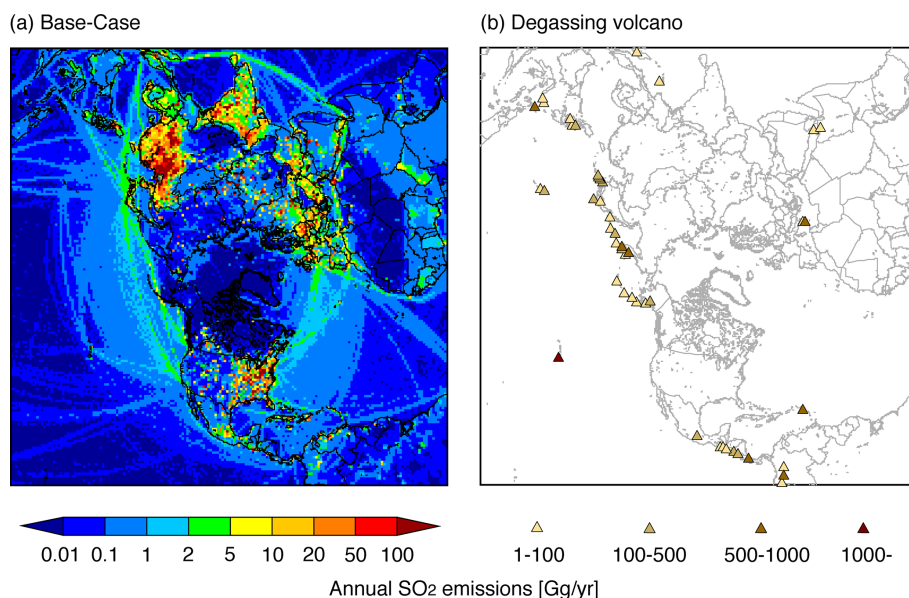
Figure 1. Geographical mapping of the **(a)** original SO$_2$ emissions used in H-CMAQ and **(b)** degassing volcanic annual SO$_2$ emissions incorporated in this study during 2010.
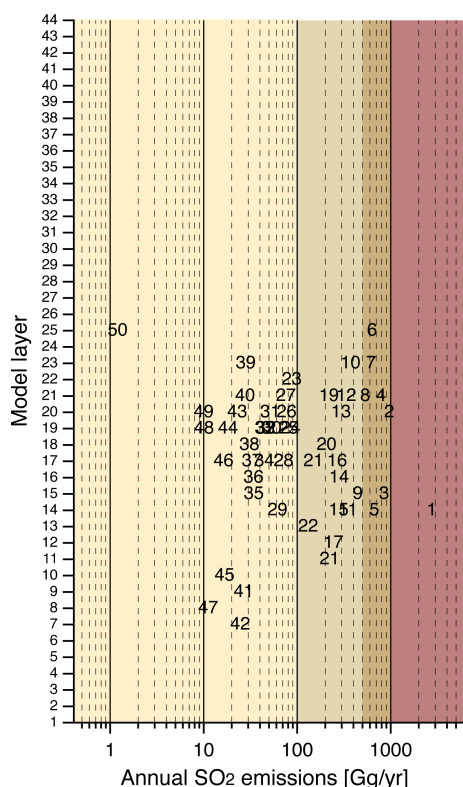

Figure 2. The model layers to which the SO$_2$ emissions from the 50 volcanoes considered in this study were assigned. See Table 1 for a listing of the volcanoes represented by each number in this figure. In Table 1, volcanoes are listed in decreasing order of their annual SO$_2$ emission amount.

(Itahashi et al., 2017a, b, 2019; Itahashi, 2018). To assess model performance in the Asian region, ground-based surface SO$_4^{2-}$ observations were obtained from the Acid Deposition Monitoring Network in East Asia (EANET) program (EANET, 2020). During 2010, filter-pack measurements of SO$_4^{2-}$ are available at 35 EANET sites with the following geographic distribution: 1 site in China, 3 sites in the South Korea, 12 sites in Japan, 2 sites in Mongolia, 4 sites in Russia, 5 sites in Thailand, 2 sites in Vietnam, 2 sites in the Philippines, 3 sites in Malaysia, and 1 site in Indonesia. Because the four-stage filter pack method in EANET measured total suspended particle, non-sea-salt (nss)-SO$_4^{2-}$ was calculated as nss-SO$_4^{2-}$ = SO$_4^{2-}$ − 0.251 × Na$^+$ in order to exclude the coarse-mode SO$_4^{2-}$ produced with sea salt. For the simplicity, nss-SO$_4^{2-}$ for EANET observation is written as SO$_4^{2-}$ throughout this article. Most of sites report two-week measurements, but some sites provide weekly or daily measurements. All available observation data were used in this study. As we have discussed in previous work (Itahashi et al., 2020a), Asian air pollution can impact on air quality over the USA; however, the magnitude of volcanic emissions on tropospheric SO$_4^{2-}$ levels over North America has not been well studied. To evaluate the impact of volcanic SO$_2$ emissions located in the Northern Hemisphere on model performance, surface observations over the USA were obtained from the Clean Air Status and Trends Network (CASTNET), which covered remote and rural sites mostly over eastern USA (CASTNET, 2020), and the Integrated Monitoring of Protected Visual Environments (IMPROVE), which covered remote sites mostly over western USA (IMPROVE, 2020). Sampling frequency is weekly and daily (1 in every 3 days)

for CASTNET and IMPROVE, respectively. A total of 84 CASTNET sites and 170 IMPROVE sites were available in 2010. Because of the coarse resolution of H-CMAQ simulations, measurements at urban sites were not considered in this study. To further examine the model's ability to represent the tropospheric sulfur distributions and budget, ambient SO$_2$ concentration at CASTNET sites and vertically integrated SO$_2$ column concentration measured by the OMI sensor were also analyzed. The OMI-measured SO$_2$ column was taken from the level-3 daily global sulfur dioxide product (OMSO2e) gridded into 0.25° (Li et al., 2020). These gridded data were mapped to the H-CMAQ modeling domain and grid structure. This product contains the total column of SO$_2$ in the planetary boundary layer (PBL) with its center of mass altitude (CMA) at 0.9 km and lacked in the vertical sensitivity. Our previous study indicated that 1 km depth for CMA in the modeled SO$_2$ column yielded best comparisons with satellite-measured SO$_2$ column over East Asia (Itahashi et al., 2017b). The observed deficit grids by satellite were also considered in the analysis of modeled SO$_2$ column. The same approach to compare and evaluate SO$_2$ column was used in this study. Furthermore, SO$_4^{2-}$ concentration in precipitation, precipitation amount, and SO$_4^{2-}$ wet deposition were also evaluated relative to observations at EANET sites over Asia and the National Atmospheric Deposition Program's National Trends Network (NADP/NTN) over the USA (NADP, 2021). Measurements by wet-only sampler are available at 49 EANET sites with daily interval at most sites and weekly or 10 d interval at others sites (EANET, 2020). Observation of volume-weighted concentration in precipitation and total weekly wet deposition are available at 240 NADP sites.

To evaluate model performance with ground-based observations, the Pearson's correlation coefficient (R) with Student's t test is used for assessing the statistical significance level. The normalized mean bias (NMB) and the normalized mean error (NME) are also calculated as follows (e.g., Zhang et al., 2006; Itahashi et al., 2020b).

$$R = \frac{\sum_1^N \left(O_i - \overline{O}\right)\left(M_i - \overline{M}\right)}{\sqrt{\sum_1^N \left(O_i - \overline{O}\right)^2}\sqrt{\sum_1^N \left(M_i - \overline{M}\right)^2}} \quad (1)$$

$$\text{NMB} = \frac{\sum_1^N \left(M_i - O_i\right)}{\sum_1^N O_i} \quad (2)$$

$$\text{NME} = \frac{\sum_1^N |M_i - O_i|}{\sum_1^N O_i}, \quad (3)$$

where N is the total observation number, O_i and M_i represent each individual observation and model result respectively, and $\overline{O}$ and $\overline{M}$ represent the arithmetical mean of observations and model results respectively. Based on a review of model performance over North America simulated by regional-scale air quality models, Emery et al. (2017) suggested threshold values of $R > 0.70$, NMB $< \pm 10\%$, and NME $< 35\%$ as performance goal, and threshold values

of $R > 0.40$, $\pm 10\% < $ NMB $< \pm 30\%$, and $35\% < $ NME $< 50\%$ as performance criteria for daily SO$_4^{2-}$.

3 Simulation results and discussion

3.1 Model evaluation

To provide an overview of the modeling results, we first present the annual-average SO$_4^{2-}$ simulated by the base H-CMAQ configuration in Fig. 3a. High concentrations of SO$_4^{2-}$ (greater than 5 µg m^{-3}; red color in Fig. 3) are noted over East Asia, some parts of India, and the Arabian Peninsula corresponding to the intense SO$_2$ emissions shown in Fig. 1. The concentrations of SO$_4^{2-}$ over Europe and USA were mostly 0.5–2.5 µg m^{-3} (blue color to green color in Fig. 3). The performance of this base case H-CMAQ simulation was evaluated over Asia and the USA through comparison with SO$_4^{2-}$ measurements by EANET, CASTNET, and IMPROVE. The results of statistical analysis using R, NMB, and NME are listed in Table 2. Detailed maps of model results over Asia and the USA with overlaid distribution of surface observations are shown in Fig. 4. Figure 4 also contains a scatterplot between base H-CMAQ and surface observations; data for each month are shown using a different color. Significant scatter is noted in the correlation between the modeled and observed concentrations with an R of 0.43 over Asia (Table 2). Recent analysis of 12 regional models participating in the MICS-Asia model intercomparison study (Chen et al., 2019) however also revealed moderate correlations (0.46–0.79) with EANET observation. In terms of NMB and NME, NMB was -37.6% and NME was 67.0% in this study (Table 2). MICS-Asia showed NMB of -19.1% as model ensemble mean but ranged from -67.0% to $+69.3\%$ for individual regional models (Chen et al., 2019). The H-CMAQ base case performance statistics were comparable or slightly worse compared to the previous regional-scale modeling studies (e.g., Itahashi, 2018; Itahashi et al., 2018; Yamaji et al., 2020; Chatani et al., 2020). This in part results from the inability of the coarse model grid resolution to resolve localized high-pollution episodes as seen in the scatterplot in Fig. 4. Over the USA, the spatial distribution patterns with low SO$_4^{2-}$ in the western USA and comparatively higher values in the eastern USA are well captured in the base H-CMAQ simulation, though the model tended to underestimate across sites in the eastern USA. The observed annual averaged values by CASTNET were ranged between 2.5 and 3.4 µg m^{-3} over eastern USA. The scatterplot also verified the reasonable correspondence between model and observations. A winter minimum and summer maximum is noted both in the modeled and observed SO$_4^{2-}$ values across the USA driven by expected variations in intensity of oxidant chemistry and conversion of S(IV) to S(VI). The statistical scores of R, NMB, and NME were within or close to the performance criteria proposed by Emery et al. (2017)

over the USA and were also comparable to previous regional-scale modeling studies (e.g., Zhang et al., 2009, 2013). Overall, despite the use of coarse horizontal grid resolution of 108 km in H-CMAQ, model performance statistics were generally within the model performance statistics noted for other the regional modeling applications. One possible contributor to the noted SO_4^{2-} underestimation over Asian region in the base H-CMAQ could be from the missing of volcanic SO_2 emissions, especially in the Pacific Rim. Comparisons of model estimated SO_2 column distributions with satellite derived values are presented in Fig. S1 in the Supplement. The R value of 0.48 indicated the general agreement for the spatial distribution pattern of SO_2 column over the Northern Hemisphere with higher concentrations in regions with high anthropogenic SO_2 emissions (illustrated in Fig. 1); however, high SO_2 column over Hawaii evident in the satellite retrieval was not captured in the base H-CMAQ simulation due to the lack of volcanic SO_2 emissions. The impact of introducing the degassing volcanic SO_2 emissions is further discussed in the following sections.

3.2 Impact of incorporating volcanic SO_2 emissions

The annual averaged SO_4^{2-} simulated after incorporating degassing volcanic SO_2 emission in H-CMAQ is shown in Fig. 3b, and the increase in concentrations relative to the base H-CMAQ is shown in Fig. 3c as absolute value and in Fig. 3d as the percentage change from the original H-CMAQ simulation. Impacts of including volcanic SO_2 emissions on tropospheric SO_4^{2-} are noted across the Pacific and up to the western coastline of the USA. It should be noted that even though the degassing volcanic emissions are allocated to upper model layers (see Fig. 2 and Table 1), they get transported through much of the troposphere with nontrivial impacts detected at the surface level. Increases of at least $0.1\,\mu g\,m^{-3}$ in SO_4^{2-} concentration were simulated except over central Asia, equatorial and high-latitude regions, and the Atlantic Ocean, and most of the USA. The maximum increase of greater than $1.0\,\mu g\,m^{-3}$ on an annual average basis was seen over the central Pacific (Fig. 3c). This increase is primarily attributed to SO_2 emission from Kilauea in Hawaii, which is estimated to have the highest degassing emissions (see Table 1). In addition, a moderate increase of up to $1.0\,\mu g\,m^{-3}$ on an annual average basis was found over the Antilles islands in the Caribbean Sea. This was related to the volcanic activity of Soufrière Hills volcano located in Montserrat (no. 5 in strength; Table 1). Compared to the broad impacts found over Pacific Rim region, the impact of incorporating degassing volcanic SO_2 emission was limited over Europe and Africa. Increased concentrations ranging between $0.1–0.3\,\mu g\,m^{-3}$ simulated over southern Europe and northern Africa region were caused by volcanoes in Italy (nos. 8 and 29 in Table 1), Ethiopia (no. 45 in Table 1), and Yemen (no. 47 in Table 1). Because only four degassing volcanoes in this region are considered in this

study (see Fig. 1b), the impact itself was lower compared to other regions. In the terms of the percentage changes relative to the original H-CMAQ (depicted in Fig. 3d), increased concentration greater than $1.0\,\mu g\,m^{-3}$ seen in Fig. 3c corresponded to $+200\%$ change, and that of $0.1\,\mu g\,m^{-3}$ corresponded to about a $+10\%$ change. Over North America and the polar region, the increased absolute concentration was less than $0.1\,\mu g\,m^{-3}$, whereas the percentage increase change was $10\%–30\%$. For the annual average, it was found that the degassing volcanic SO_2 emissions increased SO_4^{2-} concentrations less than $0.1\,\mu g\,m^{-3}$ over the entire USA, but this still represented a $10\%–20\%$ increase over the western USA.

The impacts on modeling performance by including volcanic SO_2 emissions are discussed based on the statistical analysis scores. In terms of the statistical analysis listed in Table 2, NMB and NME over Asia compared to EANET observation were improved, though the R values were not impacted significantly. This result was consistent with our previous findings that suggested volcanoes are an important source of tropospheric sulfur in East Asia (Itahashi et al., 2017a, b; Itahashi, 2018; Chatani et al., 2021). Over the USA, the base H-CMAQ had better modeling performance compared to Asia, and NMB and NME were improved when volcanic degassing emissions were included but R did not change. The improvements were noticeable in the comparison with observations at IMPROVE sites located in the western USA; NMB showed close agreement between H-CMAQ and IMPROVE observation. Both simulations of original H-CMAQ and H-CMAQ incorporating degassing SO_2 emissions showed model overestimation for ambient SO_2 concentration when compared to CASTNET observation as listed in Table S1 in the Supplement. The model performance statistics were comparable for the case incorporating degassing volcanic SO_2 emissions, indicating that additional SO_2 emissions from volcano were fully oxidized to SO_4^{2-} and thus have greater impact on changes in model performance for SO_4^{2-}. The overestimation of SO_2 could be attributed to the insufficient oxidation process from SO_2 to SO_4^{2-} in the modeling system, because SO_4^{2-} values were still underestimated by incorporating volcanic SO_2 emissions. Coarse grid resolution leading to artificial dilution of SO_2 emissions could also contribute to overestimation of predicted ambient SO_2 levels relative to measurements at remote locations. The detailed discussion using conversion rate is further presented in next Sect. 3.3. The comparison of SO_2 column with satellite observation showed the improvement of R value from 0.48 to 0.56 due to improvements in representation of the spatial variability in tropospheric SO_2 distributions resulting from capturing the high SO_2 column in the vicinity of active volcanoes such as Kilauea as illustrated in Fig. S1. The evaluation for removal processes such as wet deposition is tabulated in Table S2 in the Supplement. The base H-CMAQ simulation tended to underestimate both SO_4^{2-} concentration in precip-
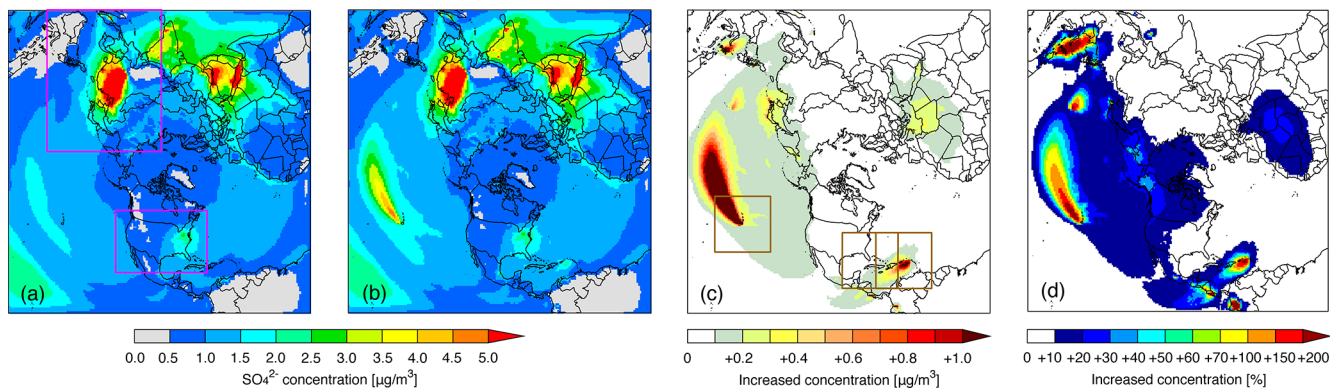
Figure 3. Simulated annual averaged SO$_4^{2-}$ concentration in 2010 by **(a)** original H-CMAQ and **(b)** H-CMAQ with incorporation of volcanic SO$_2$ emissions, **(c)** increased concentration by the incorporation of volcanic SO$_2$ emissions, and **(d)** same as **(c)** but shown as relative percentages at the surface. The rectangular regions colored in pink in **(a)** indicate the Asia (top left) and USA (bottom right) subdomains used for detailed analysis. The rectangular regions colored in brown in **(c)** indicate areas for the analysis on specific site analysis that were largely impacted by degassing SO$_2$ volcanoes.

Table 2. Statistical analysis of modeled SO$_4^{2-}$ concentration with observations.

	N	Mean		R	NMB	NME
		Observation	Model			
EANET						
original H-CMAQ	1167	3.68	2.30	0.43[c]	−37.6 %	67.0 %
incorporation of volcanic emissions			2.44	0.43[c]	−33.6 %	66.0 %
CASTNET						
original H-CMAQ	4216	1.91	1.36	0.73[c]	−28.7 %	39.4 %
incorporation of volcanic emissions			1.42	0.73[c]	−25.6 %	38.6 %
IMPROVE						
original H-CMAQ	18 844	1.05	0.94	0.64[c]	−10.6 %	53.9 %
incorporation of volcanic emissions			1.02	0.64[c]	−3.2 %	46.0 %

Note: The unit of mean for observations and simulations is µg m^{-3}. Suggested threshold values of $R > 0.70$, NMB $< \pm 10$ %, and NME < 35 % as performance goal, and threshold values of $R > 0.40$, ± 10 % $<$ NMB $< \pm 30$ %, and 35 % $<$ NME < 50 % as performance criteria for daily SO$_4^{2-}$ by the regional-scale modeling reviewed by Emery et al. (2017). Significance levels by Student's t test for correlation coefficients between observations and simulations are remarked as [a] $p < 0.05$, [b] $p < 0.01$, and [c] $p < 0.001$, and lack of a mark indicates no significance.

itation and wet deposition. The inclusion of volcanic SO$_2$ emission sources led to slight improvements in the NMB and R, but the NME was largely unaltered. From these evaluations, it is concluded that the incorporation of degassing volcanic SO$_2$ emissions helps to improve performance of simulated SO$_4^{2-}$ in H-CMAQ by a small margin.

The impacts of degassing volcanic SO$_2$ emissions on seasonal SO$_4^{2-}$ distributions and long-range transport were further analyzed by examining monthly mean contributions as illustrated in Fig. 5. Similar to the annual mean distributions shown in Fig. 3c, the maximum impact was seen over the central Pacific associated with emissions from the Kilauea volcano throughout the year. Regarding its monthly variation, the increased concentrations at the surface level

during spring to summer season (from April to September) were higher than those during winter (especially, December and January). The higher impacts during summer result both from higher rates of SO$_2$ to SO$_4^{2-}$ conversion as well as enhanced convective mixing. In contrast during winter lower conversion rates and a more stably stratified atmosphere result in reduced SO$_4^{2-}$ from volcanic emissions at the surface. The enhanced SO$_4^{2-}$ associated with emissions from the Kilauea volcano (with highest emission rate as indicted in Table 1) stretches across the central Pacific to the western shores of the USA, with enhancements in surface-level SO$_4^{2-}$ on a monthly-mean basis greater than 0.1 µg m^{-3} across portions of the western USA. The contributions of volcanoes
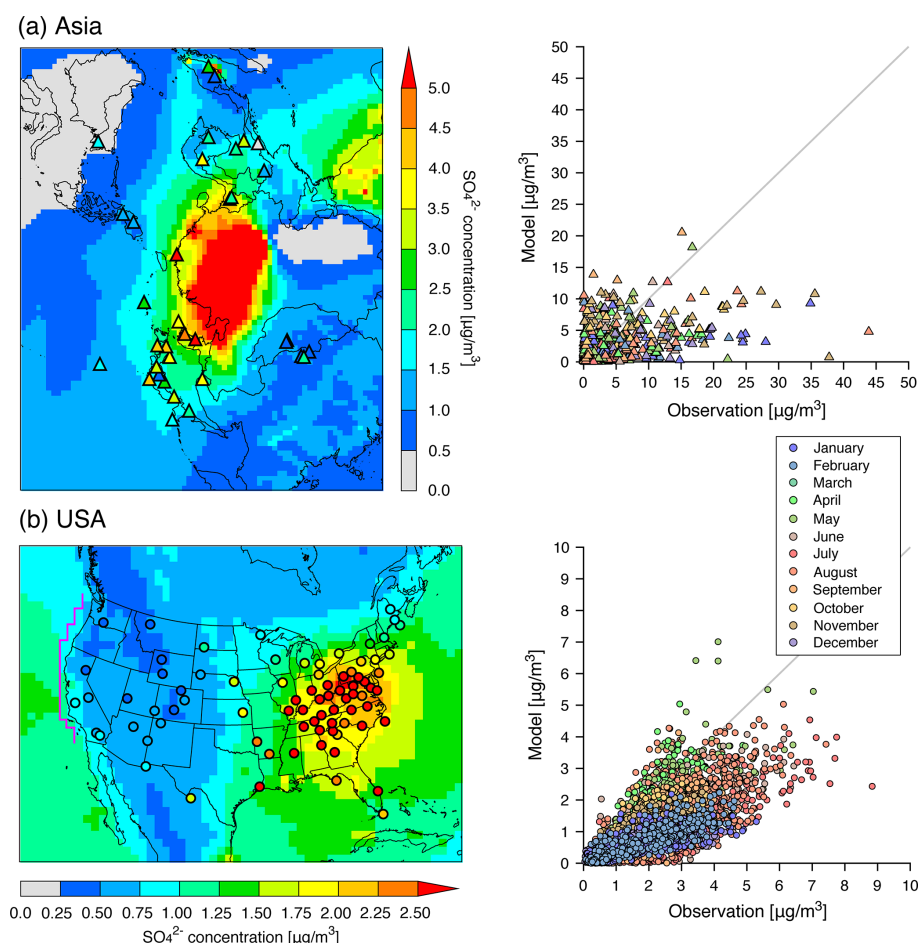
Figure 4. Simulated annual averaged SO$_4^{2-}$ concentration in 2010 by original H-CMAQ over **(a)** Asia and **(b)** USA with overlaid EANET and CASTNET surface observations. Scatterplots between surface observation (EANET over Asia, and CASTNET over USA) and original H-CMAQ with identification colors for each month are also shown. Note that the color scale is different for Asia and USA. The pink line over the western USA in **(b)** is the defined as the western edge to analyze the vertical profile of SO$_4^{2-}$ concentrations (see Fig. 7).

located on the Kamchatka Peninsula (nos. 2, 6, 12, 14, 16, 19, and others in Table 1) are estimated to be comparatively lower on an annual average basis but may be higher episodically under conducive transport condition. During the winter season, the impacts from Kilauea did not reach the western USA; however, the impacts from Soufrière Hills located in Montserrat (no. 5 in Table 1) reached the southern USA. Further analysis focused on specific sites is discussed in next section.

3.3 Impacts of volcanic SO$_2$ emissions at specific sites

Detailed analysis at an observation site located in Hawaii was further conducted to evaluate model performance. According to the observation summary (WRAP, 2020), a large fraction of the measured SO$_4^{2-}$ at this location is attributed to SO$_2$ emissions associated with volcanic activity from Kilauea. A total of three IMPROVE sites are located in the state of Hawaii. One of the sites is located in the Hawaii

Volcanoes National Park and is in the vicinity of the Kilauea volcano (site name is HAVO1). Comparison of model and observed temporal variation in SO$_4^{2-}$ at this site is displayed in Fig. 6a. The observation showed higher concentration during the winter season, and the average concentration through 2010 was 2.37 µg m^{-3}. The base H-CMAQ simulation showed largely invariant concentrations throughout the year with an annual average value of 0.87 µg m^{-3} and a negative correlation against observation. The statistical scores of NMB showed high negative bias because the base H-CMAQ did not capture the higher concentration observed during winter. By including the degassing volcano emissions, the model showed spikes for higher concentration days. Though the observed maximum peak of 30 µg m^{-3} on 3 January was not fully captured, the simulated values of around 10 µg m^{-3} by incorporating the volcano emissions were significantly enhanced relative to the base model. The result showed that the averaged concentration was 2.87 µg m^{-3}, and NMB showed +21.2 % with moderate correlation by R of 0.36.
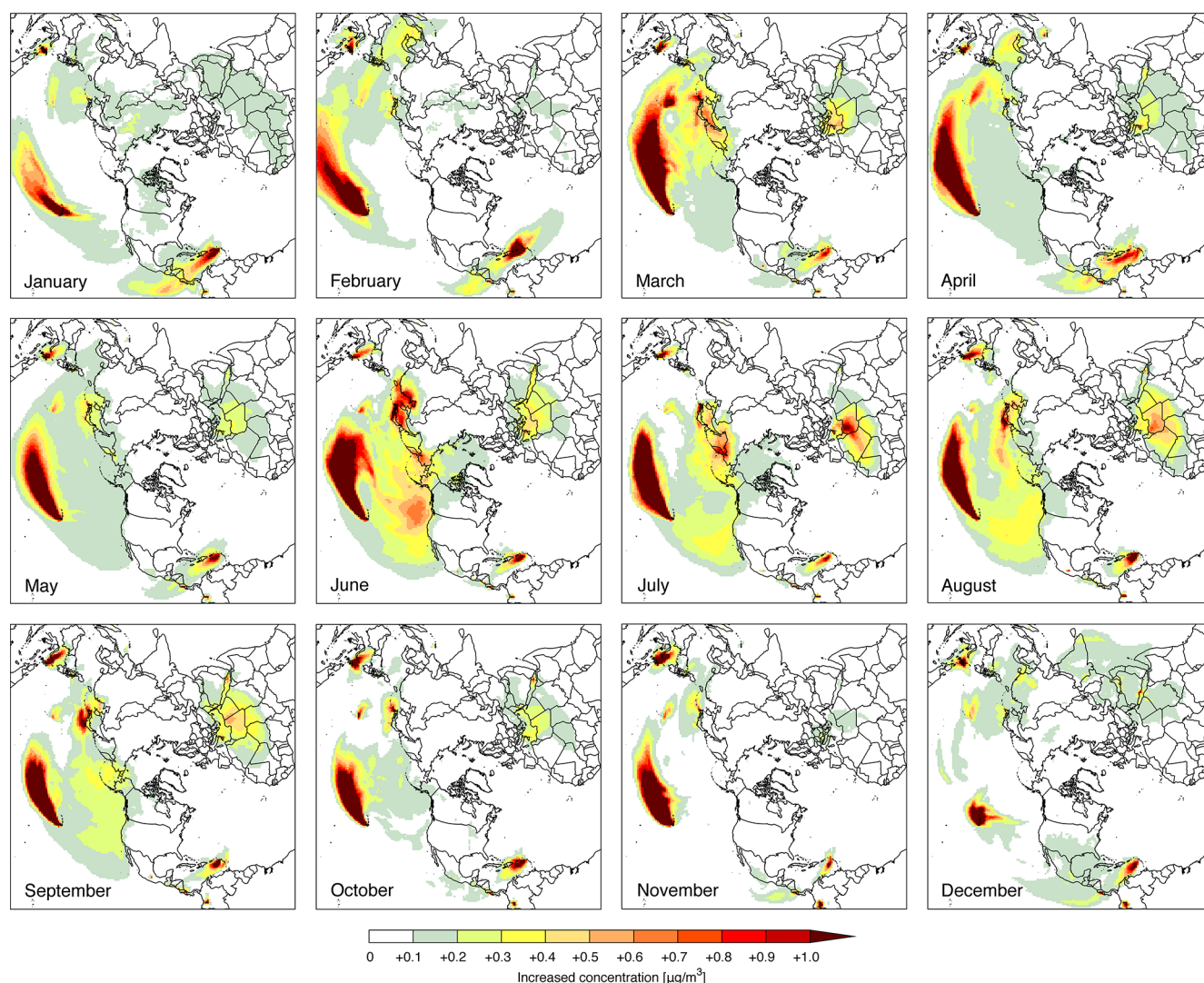
Figure 5. Simulated increased surface SO$_4^{2-}$ concentration by the incorporation of volcanic SO$_2$ emissions over each month in 2010 at surface.

The inclusion of degassing volcanoes led to better performance at this specific site; however, the deterioration in the value of NME should be considered. While the H-CMAQ simulations with incorporated volcanoes also showed lower SO$_4^{2-}$ concentrations during summer season compared to winter, the simulated summertime values were higher than observed and led to a persistent positive bias during this season. A potential reason for this behavior could be the treatment of degassing volcanoes SO$_2$ emissions as a constant flux in this study. For example, a case study targeted to quantify the air quality impacts of the Kilauea eruption in 2018 showed the importance of temporal variation of emissions and plume rise calculation (Tang et al., 2020). Our results indicate general improvements of model performance by including degassing volcano emissions represented by a constant temporal and vertical profile, but refining the treatment

of these aspects should be studied in future work. In terms of SO$_2$ concentration, IMPROVE sites do not measure it. Based on an intensive observational study at Kilauea during January and February 2013, SO$_2$ concentrations showed large variations from below 1 ppbv under conditions of no influence of the volcanic plume to over 3000 ppbv when air masses influenced by the volcanic plume were sampled (Kroll et al., 2015). In the base H-CMAQ calculation, the daily averaged SO$_2$ mixing ratios for the grid cell with the Kilauea volcano ranged from below 0.01 to 0.14 ppbv, while the annual mean value was 0.03 ppbv. In contrast, when volcanic emissions were incorporated in H-CMAQ, simulated SO$_2$ mixing ratios ranged from below 0.03 to 1088.20 ppbv with an annual mean value of 221.08 ppbv, which better matches the dynamic range inferred from the SO$_2$ measurements in the vicinity of the Kilauea volcano reported in Kroll et al. (2015).
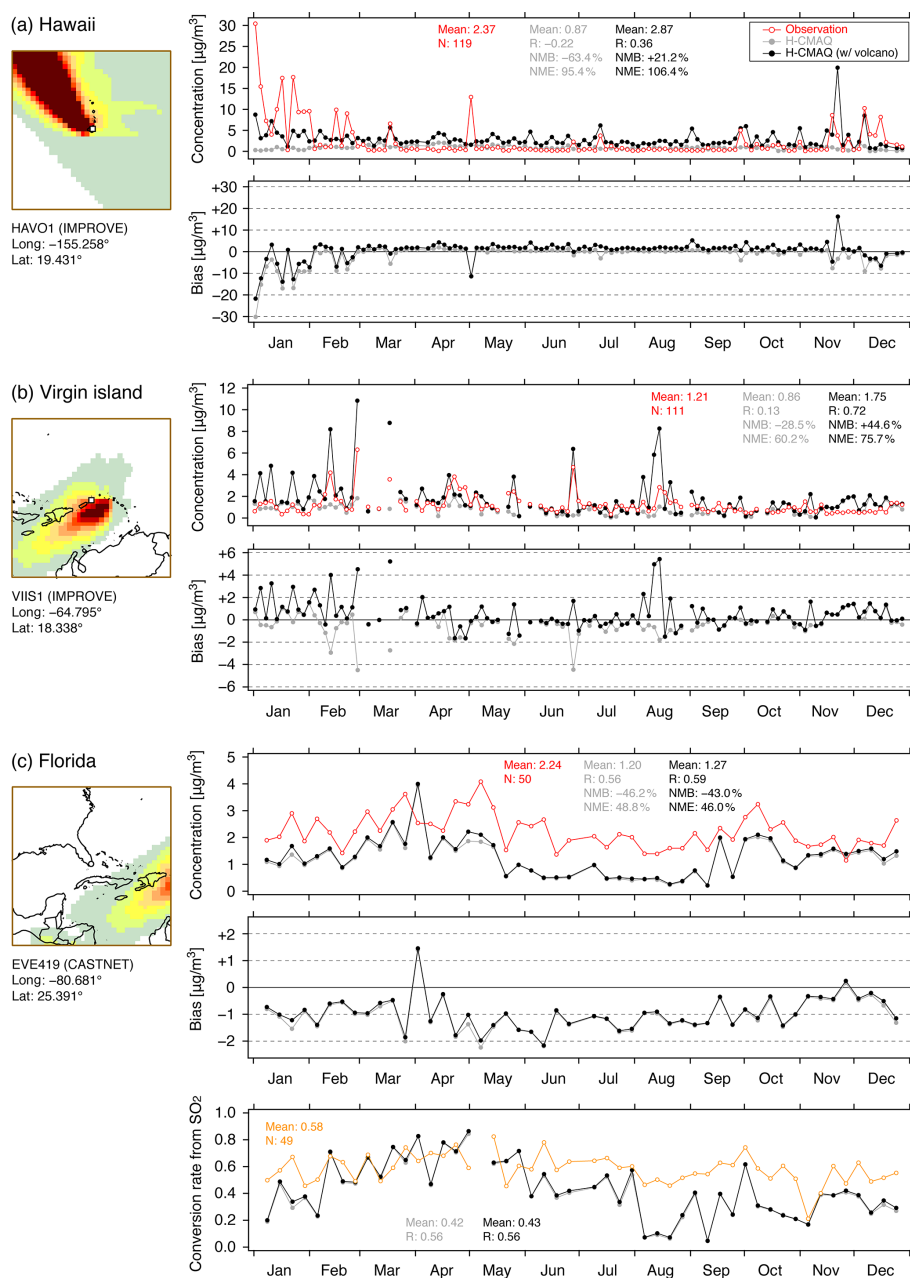
Figure 6. Temporal variation of observed and simulated SO$_4^{2-}$ concentrations and simulation biases at **(a)** Hawaii IMPROVE site (HAVO1), **(b)** Virgin Islands IMPROVE site (VIIS1), and **(c)** Florida CASTNET site (EVE419) in 2010. Red open circle denotes observations, and gray and black closed circles denote original H-CMAQ and H-CMAQ incorporating volcanoes, respectively. Statistical scores are indicated in the inset. The comparison of conversion rate from SO$_2$ to SO$_4^{2-}$ is also shown in **(c)**.

A second location-specific analysis was conducted at a site located in the Virgin Islands and in the state of Florida. As seen in the monthly-average spatial distribution patterns (Fig. 5), the influence of volcanic activity of Soufrière Hills located in Montserrat is more prominent during winter. The nearest observation site from Soufrière Hills is the IMPROVE site VIIS1, and the southernmost measurement location in Florida (see Fig. 4) is the CASTNET site

EVE419 and comparison of modeled values with observations at these locations is shown in Fig. 6b and c. At VIIS1 (Fig. 6b), the base H-CMAQ simulation showed invariant concentrations throughout the year with an annual average value of 0.86 µg m^{-3}. The statistical scores of R showed scattered correspondence between model and observation; NMB showed negative bias because the base H-CMAQ did not capture the episodical peak concentration. By including the de-

gassing volcanic SO$_2$ emissions, the model caught episodical peak events. The statistical scores showed that the averaged concentration was 1.75 µg m^{-3}, and NMB showed +44.6 %, and R was dramatically improved to 0.72. The deterioration in the value of NME was found because of the continuous model overestimation. As also suggested for the case in Hawaii, further refinement on emission treatments is required. At EVE419 (Fig. 6c), the seasonal pattern with summer minima was captured by H-CMAQ but underestimated throughout the year. Increased concentrations through the incorporation of volcanic emissions are noted during January, late April to early May, and December. The increase during late April to early May was not seen from the monthly averaged spatial distribution (Fig. 5); hence these could be the episodic long-range transport by southeasterly winds. Because of these increased concentrations, all statistical scores of R, NMB and NME showed improvement compared to the base H-CMAQ. CASTNET also provides measurements of weekly-average SO$_2$ mixing ratios, which are used to evaluate the model's performance for SO$_2$ prediction, as shown in Table S1. In addition to domain-mean evaluation, we evaluated SO$_2$ at the EVE419 site in Florida. At this site, the observed annual mean was 0.61 ppbv, whereas base H-CMAQ and H-CMAQ with volcanic SO$_2$ emissions both showed 0.77 ppbv. Additionally, the results suggest that the SO$_2$ from volcanic sources was fully oxidized to SO$_4^{2-}$ during long-range transport, and there was no direct transport of SO$_2$ itself at this site. At this CASTNET site of EVE419 at Florida, the conversion rate from SO$_2$ to SO$_4^{2-}$ was further examined. This conversion rate is defined as SO$_4^{2-}$/(SO$_4^{2-}$ + SO$_2$), and a higher value indicates the oxidation from SO$_2$ to SO$_4^{2-}$. The temporal variation of conversion rate is also plotted in Fig. 6b. The conversion rate was lower in the cold season and higher in the warm season, and this general feature was captured by model. The mean of conversion rate throughout the year was 0.58 in the observation, whereas original H-CMAQ was 0.42. By incorporating degassing volcanic SO$_2$ emissions, the mean of conversion rate increased in 0.43 but still underestimated the observed value. Since data from routine measurement networks are not designed to specifically characterize impacts of volcanic emissions on atmospheric sulfur budgets, these observations are unable to unambiguously quantify any modulation in S(IV) to S(VI) conversion rates due to the presence of volcanic emissions as also evidenced by the small change in the estimated conversion rate between the simulations with and without volcanic degassing emissions. Collectively, these results and those summarized in Table 2 and Fig. 4 suggest that inclusion of degassing volcanic emissions moderately improves model performance statistics for simulated SO$_4^{2-}$ spatial distributions and temporal variations. Note that the incorporation of volcanic degassing emissions does not necessarily improve model performance in all instances due to the presence of uncertainties and potentially compensating errors in other parts of the

modeling system (i.e., model input fields like other emissions and meteorology, model representation of processes such as chemical reactions and deposition) and suitability of the measurement network (e.g., proximity) in characterizing the variability in tropospheric composition due to volcanic degassing emissions. Nonetheless, incorporating the degassing volcanic SO$_2$ emissions which clearly occur in nature is an important aspect for enhancing the completeness of the modeling system itself. Quantifying the space and time variations of persistent volcanic degassing emissions on tropospheric composition is important, especially in the context of using models to characterize background pollution levels and anthropogenic enhancements of tropospheric pollutants and associated health and visibility impacts.

3.4 Impact on upper troposphere

Finally, the impacts caused by including the degassing volcanoes were investigated throughout the troposphere. In a subsequent analysis, the boundary layer is defined from the surface to 750 hPa, and the free troposphere is defined from 750 to 250 hPa, and pressure levels of 750, 500, and 250 hPa are used to refer to the bottom, middle, and top of the free troposphere similar to our previous study (Itahashi et al., 2020a). The vertical profile of simulated SO$_4^{2-}$ concentration averaged along the edge of western USA (defined in Fig. 4b) was analyzed. The vertical profile of the base H-CMAQ and the increased concentration due to incorporating the degassing volcanic SO$_2$ emission are plotted in Fig. 7. Modeled SO$_4^{2-}$ concentrations decreased from the surface to upper layers, and concentration levels were greater in summer than those during winter (e.g., Fig. 4 for surface results). Incorporation of volcanic SO$_2$ emissions increased monthly mean SO$_4^{2-}$ within the boundary layer by up to 0.4 µg m^{-3} during June to September. This increase is consistent with the spatial distribution at surface depicted in Fig. 5, but it also occurs through the depth of the boundary layer. During other months, the simulated concentration increases were less than 0.1 µg m^{-3} throughout the free troposphere.

Simulated annual average SO$_4^{2-}$ concentration distributions at the bottom, middle, and top of the free troposphere from the two model simulations and the estimated increase due to incorporation of degassing volcanic emissions are shown in Fig. 8. The simulated spatial distribution of SO$_4^{2-}$ exhibited similar patterns at the bottom of the free troposphere (Fig. 8a and d) with higher concentration over Asian region. However, significant differences in the magnitude and spatial distributions of simulated SO$_4^{2-}$ between the two simulations are noted at the middle and top of the free troposphere as seen from higher concentration in the North Pacific region close to the North Pole (Fig. 8b, c, e, and f). The maximum concentrations at the top of the free troposphere (Fig. 8c and f) decreased by a factor of 10 compared to those at the surface (Fig. 3a and b). The increased concentration by including degassing volcanoes showed the in-
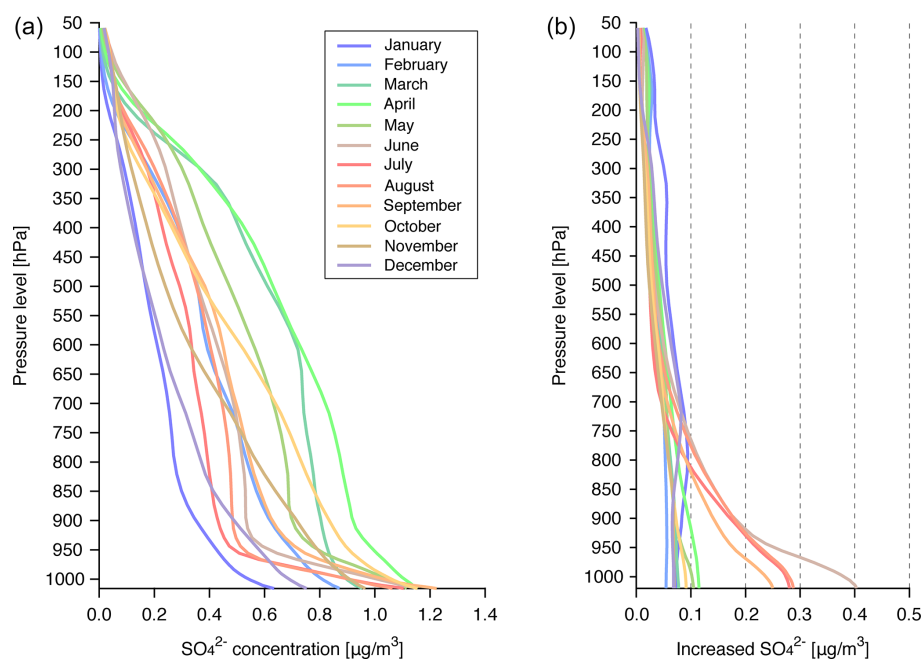
Figure 7. Vertical profile of simulated SO$_4^{2-}$ concentration of each month in 2010 at the edge of western USA (see Fig. 4): **(a)** original H-CMAQ and **(b)** increased concentration by the incorporation of volcanic SO$_2$ emissions.

crement corresponded to the location of volcanoes. In contrast to the increased concentrations over the Pacific Rim region found at the surface level (Fig. 3c), increased SO$_4^{2-}$ over the Bering Sea was noticeable at the bottom of the free troposphere (Fig. 8g). Over this area, increased SO$_4^{2-}$ values ranging from +0.08 to +0.2 at the bottom of free troposphere were found. This is mainly caused by the Mutnovsky, Gorely, Kliuchevskoi (Klyuchevskoi), and Bezymianny volcanoes (nos. 5 and 6 in Table 1), other volcanoes located on the Kamchatka Peninsula (nos. 12, 14, 16, 19, 24, 35, 36, and 48), and volcanoes over the Alaska Peninsula (nos. 37–40, and 46) in the surrounding Bering Sea. These volcanoes were characterized by the relatively higher altitude (no. 6 was allocated into the highest altitude) considered in this study (Table 1 and Fig. 2). The increased concentrations at the middle and top of the free troposphere were widely distributed with centering on the North Pole. These increased concentrations indicated that while volcanic emissions were assumed to be injected into the lower and middle free troposphere (Fig. 2), their impacts on secondary SO$_4^{2-}$ production were detected throughout the free troposphere. Based on the percentage change relative to the original H-CMAQ simulation, Fig. 8 further shows that the spatial extent of the impact of including degassing volcanic SO$_2$ emissions on SO$_4^{2-}$ increased with height, with most of the Northern Hemisphere showing increases exceeding 10 % at 250 hPa.

4 Conclusions

Previous work on the development and evaluation of the H-CMAQ model has historically not considered volcanic SO$_2$ emissions. In this study, satellite-constrained SO$_2$ emissions from 50 degassing volcanoes over the Northern Hemisphere are incorporated into H-CMAQ, and their impacts on tropospheric SO$_4^{2-}$ are evaluated for model simulations of the calendar year 2010. Model performance was evaluated using network observations of EANET over Asia and CASTNET and IMPROVE over the USA. The base H-CMAQ underestimated SO$_4^{2-}$, and this was partially rectified by incorporating volcanic SO$_2$ emissions as indicated through improvements in the statistical scores of R, NMB, and NME. Over Asia, the largest increases in SO$_4^{2-}$ were simulated in the vicinity of the volcanoes, especially over Japan and Indonesia. Over the USA, the largest impact over the central Pacific was caused by including the Kilauea volcano, and its impacts on the continental USA were limited to the western USA during the summer. The emissions from the Soufriére Hills volcano located in Montserrat affected the southern USA during the winter season. Analysis of temporal variations at measurement sites located in Hawaii, the Virgin Islands, and Florida showed improvements in modeling performance as a result of the inclusion of volcanic SO$_2$ emissions. The changes in simulated aloft SO$_4^{2-}$ concentration were investigated, and it was revealed that the impacts were detected up to the top of the free troposphere, although the considered SO$_2$ emissions were injected in the lower and middle of the free troposphere.
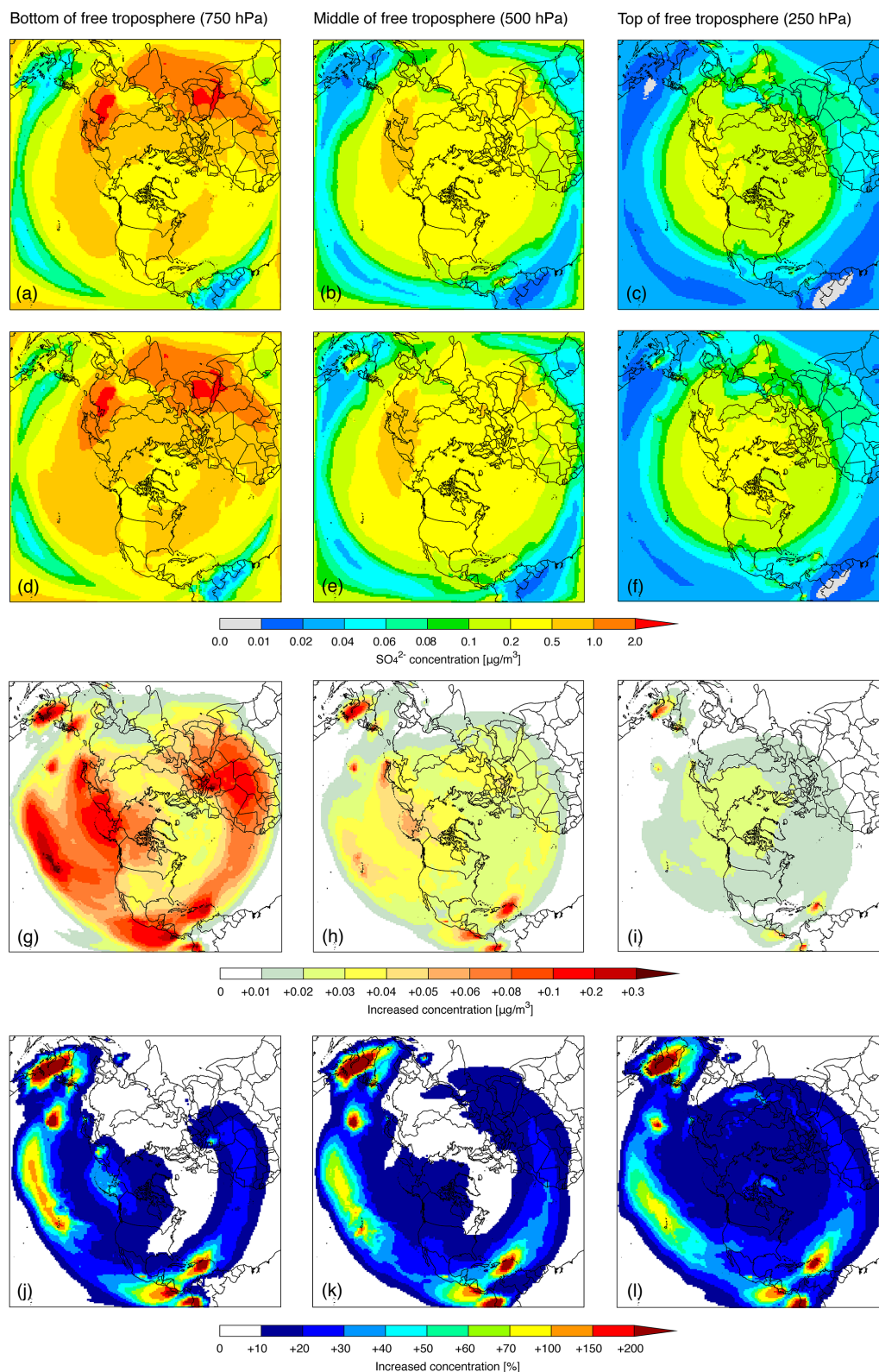
Figure 8. Simulated annual averaged SO$_4^{2-}$ concentration in 2010 by **(a–c)** original H-CMAQ and **(d–f)** H-CMAQ with incorporation of volcanic SO$_2$ emissions, **(g–i)** increased concentration by the incorporation of volcanic SO$_2$ emissions, and **(j–l)** same as **(g–i)** but shown as relative percentage at the bottom of the free troposphere (750 hPa; **a**, **d**, **g**, **j**), middle of the free troposphere (500 hPa; **b**, **e**, **h**, **k**), and top of the free troposphere (250 hPa; **c**, **f**, **i**, **l**).

The results suggest that emission of SO_2 resulting from volcanic degassing is one of the important sources that should be considered in the modeling system as it regulates tropospheric SO_4^{2-} levels not only in the vicinity of the volcano but also through long-range transport that modulates background levels at downwind continents. In addition to inclusion of persistent degassing emissions, eruptive volcanic emissions can also play an important role in episodically modulating tropospheric sulfur budgets and radiative forcing (Schmidt et al., 2012, 2018). As seen from the analysis of model and measured values at the Kilauea volcanic site in this study, the approach to treat the degassing volcanic SO_2 emissions as assigned in one model vertical layer without any temporal variation sometimes leads to the unexpected positive bias on cleaner days. A more realistic treatment of temporal variation of degassing gases and the related meteorological parameters (e.g., local wind speed) would be useful to further refine the modeling performance of SO_4^{2-} produced via volcanic SO_2 emission.

References

Acid Deposition Monitoring Network in East Asia (EANET): Homepage, available at: http://www.eanet.asia/, last access: 1 September 2020.

Andres, R. J. and Kasgnoc, A. D.: A time-averaged inventory of subaeroal volcanic sulfur emissions, J. Geophys. Res., 103, 25251–25261, 1998.

Appel, K. W., Napelenok, S. L., Foley, K. M., Pye, H. O. T., Hogrefe, C., Luecken, D. J., Bash, J. O., Roselle, S. J., Pleim, J. E., Foroutan, H., Hutzell, W. T., Pouliot, G. A., Sarwar, G., Fahey, K. M., Gantt, B., Gilliam, R. C., Heath, N. K., Kang, D., Mathur, R., Schwede, D. B., Spero, T. L., Wong, D. C., and Young, J. O.: Description and evaluation of the Community Multiscale Air Quality (CMAQ) modeling system version 5.1, Geosci. Model Dev., 10, 1703–1732, https://doi.org/10.5194/gmd-10-1703-2017, 2017.

Carn, S. A., Clarisse, L., and Prata, A. J.: Multidecadal satellite measurements of global volcanic degassing, J. Volcanol. Geoth. Res., 311, 99–134, https://doi.org/10.1016/j.volgeores.2016.01.002, 2016.

Carn, S. A., Fioletov, V. E., McLinden, C. A., Li, C., and Krotkov, N. A.: A decade of global volcanic SO_2 emissions measured from space, Sci. Rep., 7, 44095, https://doi.org/10.1038/srep44095, 2017.

Chatani, S., Shimadera, H., Itahashi, S., and Yamaji, K.: Comprehensive analyses of source sensitivities and apportionments of PM$_{2.5}$ and ozone over Japan via multiple numerical techniques, Atmos. Chem. Phys., 20, 10311–10329, https://doi.org/10.5194/acp-20-10311-2020, 2020.

Chatani, S., Itahashi, S., and Yamaji, K.: Advantages of continuous monitoring of hourly PM$_{2.5}$ component concentrations in Japan for modeli validation and source sensitivity analyses, Asian Journal of Atmospheric Environment, 15, 2021008, https://doi.org/10.5572/ajae.2021.008, 2021.

Chen, L., Gao, Y., Zhang, M., Fu, J. S., Zhu, J., Liao, H., Li, J., Huang, K., Ge, B., Wang, X., Lam, Y. F., Lin, C.-Y., Itahashi, S., Nagashima, T., Kajino, M., Yamaji, K., Wang, Z., and Kurokawa, J.: MICS-Asia III: multi-model comparison and evaluation of aerosol over East Asia, Atmos. Chem. Phys., 19, 11911–11937, https://doi.org/10.5194/acp-19-11911-2019, 2019.

Chin, M. and Jacob, D. J.: Anthropogenic and natural contributions to tropospheric sulfate: A global model analysis, J. Geophys. Res.-Atmos., 101, 18691–18699, 1996.

Chin, M., Jacob, D. J., Gardner, G. M., Foreman-Fowler, M. S., Spiro, P. A., and Savoie D. L.: A global three-dimensional model of tropospheric sulfate, J. Geophys. Res.-Atmos., 101, 18667–18690, 1996.

Clean Air Status and Trends Network (CASTNET), US Environmental Protection Agency Clean Air Markets Division: Homepage, available at: https://www.epa.gov/castnet, last access: 1 September 2020.

Emery, C., Liu, Z., Russell, A. G., Odman, M. T., Yarwood, G., and Kumar, N.: Recommendations on statistics and benchmarks to assess photochemical model performance, JAPCA J. Air Waste Ma., 67, 582–598, https://doi.org/10.1080/10962247.2016.1265027, 2017.

Galmarini, S., Koffi, B., Solazzo, E., Keating, T., Hogrefe, C., Schulz, M., Benedictow, A., Griesfeller, J. J., Janssens-Maenhout, G., Carmichael, G., Fu, J., and Dentener, F.: Technical note: Coordination and harmonization of the multi-scale, multi-model activities HTAP2, AQMEII3, and MICS-Asia3: simulations, emission inventories, boundary conditions, and model output formats, Atmos. Chem. Phys., 17, 1543–1555, https://doi.org/10.5194/acp-17-1543-2017, 2017.

Gan, C.-M., Pleim, J., Mathur, R., Hogrefe, C., Long, C. N., Xing, J., Wong, D., Gilliam, R., and Wei, C.: Assessment of long-term WRF–CMAQ simulations for understanding direct aerosol effects on radiation "brightening" in the United States, Atmos. Chem. Phys., 15, 12193–12209, https://doi.org/10.5194/acp-15-12193-2015, 2015.

Ge, C., Wang, J., Carn, C., Yang, K., Ginoux, P., and Krotkov, N.: Satellite-based global volcanic SO$_2$ emissions and sulfate direct radiative forcing during 2005–2012, J. Geophys. Res.-Atmos., 121, 3446–3464, https://doi.org/10.1002/2015JD023134, 2016.

Hand, J. L., Schichtel, B. A., Malm, W. C., and Pitchford, M. L.: Particulate sulfate ion concentration and SO$_2$ emission trends in the United States from the early 1990s through 2010, Atmos. Chem. Phys., 12, 10353–10365, https://doi.org/10.5194/acp-12-10353-2012, 2012.

Hogrefe, C., Liu, P., Pouliot, G., Mathur, R., Roselle, S., Flemming, J., Lin, M., and Park, R. J.: Impacts of different characterizations of large-scale background on simulated regional-scale ozone over the continental United States, Atmos. Chem. Phys., 18, 3839–3864, https://doi.org/10.5194/acp-18-3839-2018, 2018.

Iacono, M. J., Delamere, J. S., Mlawer, E. J., Shephard, M. W., Clough, S. A., and Collins, W. D.: Radiative forcing by long-lived greenhouse gases: Calculations with the AER radiative transfer models, J. Geophys. Res., 113, D13103, https://doi.org/10.1029/2008JD009944, 2008.

Integrated Monitoring of Protected Visual Environments (IMPROVE): Homepage, available at: http://vista.cira.colostate.edu/Improve, last access: 1 September 2020.

Itahashi, S.: Toward synchronous evaluation of source apportionments for atmospheric concentration and deposition of sulfate aerosol over East Asia, J. Geophys. Res.-Atmos., 123, 2927–2953, https://doi.org/10.1002/2017JD028110, 2018.

Itahashi, S., Hatakeyama, S., Shimada, K., Tatsuta, S., Taniguchi, Y., Chan, C. K., Kim, Y. P., Lin, N.-H., and Takami, A.: Model estimation of sulfate aerosol source collected at Cape Hedo during an intensive campaign in October–November, 2015, Aerosol Air Qual. Res., 17, 3079–3090, https://doi.org/10.4209/aaqr.2016.12.0592, 2017a.

Itahashi, S., Hayami, H., Yumimoto, K., and Uno, I.: Chinese province-scale source apportionments for sulfate aerosol in 2005 evaluated by the tagged tracer method, Environ. Pollut., 220, 1366–1375, 2017b.

Itahashi, S., Yamaji, K., Chatani, S., and Hayami, H.: Refinement of modeled aqueous-phase sulfate production via the Fe- and Mn-catalyzed oxidation pathway, Atmosphere, 9, 132, https://doi.org/10.3390/atmos9040132, 2018.

Itahashi, S., Hatakeyama, S., Shimada, K., and Takami, A.: Sources of high sulfate aerosol concentration observed at Cape Hedo in spring 2012, Aerosol Air Qual. Res., 19, 587–600, https://doi.org/10.4209/aaqr.2018.09.0350, 2019.

Itahashi, S., Mathur, R., Hogrefe, C., Napelenok, S. L., and Zhang, Y.: Modeling stratospheric intrusion and trans-Pacific transport on tropospheric ozone using hemispheric CMAQ during April 2010 – Part 2: Examination of emission impacts based on the higher-order decoupled direct method, Atmos. Chem. Phys., 20, 3397–3413, https://doi.org/10.5194/acp-20-3397-2020, 2020a.

Itahashi, S., Mathur, R., Hogrefe, C., and Zhang, Y.: Modeling stratospheric intrusion and trans-Pacific transport on tropospheric ozone using hemispheric CMAQ during April 2010 – Part 1: Model evaluation and air mass characterization for stratosphere–troposphere transport, Atmos. Chem. Phys., 20, 3373–3396, https://doi.org/10.5194/acp-20-3373-2020, 2020b.

Janjic, Z.: The step-mountain Eta coordinate Model: Further developments of the convection, viscous sublayer, and turbulence closure schemes, Mon. Weather Rev., 122, 927–945, 1994.

Janssens-Maenhout, G., Crippa, M., Guizzardi, D., Dentener, F., Muntean, M., Pouliot, G., Keating, T., Zhang, Q., Kurokawa, J., Wankmüller, R., Denier van der Gon, H., Kuenen, J. J. P., Klimont, Z., Frost, G., Darras, S., Koffi, B., and Li, M.: HTAP_v2.2: a mosaic of regional and global emission grid maps for 2008 and 2010 to study hemispheric transport of air pollution, Atmos. Chem. Phys., 15, 11411–11432, https://doi.org/10.5194/acp-15-11411-2015, 2015.

Kain, J. S.: The Kain-Fritsch convective parameterization: An update, J. Appl. Meteorol., 43, 170–181, 2004.

Kroll, J. H., Cross, E. S., Hunter, J. F., Pai, S., XII, T., XI, T., Wallace, L. M. M., Croteau, P. L., Jayne, J. T., Worsnop, D. R., Heald, C. L., Murphy, J. G., and Frankel, S. L.: Atmospheric evolution of sulfur emissions from Kilauea: Real-time measurements of oxidation, dilution, and neutralization within a volcanic plume, Environ. Sci. Technol., 49, 4129–4137, https://doi.org/10.1021/es506119x, 2015.

Lamotte, C., Guth, J., Marécal, V., Cussac, M., Hamer, P. D., Theys, N., and Schneider, P.: Modeling study of the impact of SO$_2$ volcanic passive emissions on the tropospheric sulfur budget, Atmos. Chem. Phys., 21, 11379–11404, https://doi.org/10.5194/acp-21-11379-2021, 2021.

Li, C., Krotkov, N. A., and Leonard, P.: OMI/Aura Sulfur Dioxide (SO2) Total Column L3 1 day Best Pixel in 0.25 degree x 0.25 degree V3, Greenbelt, MD, USA, Goddard Earth Sciences Data and Information Services Center (GES DISC) [data set], https://doi.org/10.5067/Aura/OMI/DATA3008, 2020.

Li, M., Liu, H., Geng, G., Hong, C., Liu, F., Song, Y., Tong, D., Zheng, B., Cui, H., Man, H., Zhang, Q., and He, K.: Anthropogenic emission inventories in China: a review, Natl. Sci. Rev., 4, 834–866, 2017.

Liu, J., Mauzerall, D. L., and Horowitz, L. W.: Source-receptor relationships between East Asian sulfur dioxide emissions and Northern Hemisphere sulfate concentrations, Atmos. Chem. Phys., 8, 3721–3733, https://doi.org/10.5194/acp-8-3721-2008, 2008.

Mathur, R., Xing, J., Gilliam, R., Sarwar, G., Hogrefe, C., Pleim, J., Pouliot, G., Roselle, S., Spero, T. L., Wong, D. C., and Young, J.: Extending the Community Multiscale Air Quality (CMAQ) modeling system to hemispheric scales: overview of process considerations and initial applications, Atmos. Chem. Phys., 17, 12449–12474, https://doi.org/10.5194/acp-17-12449-2017, 2017.

Mathur, R., Zhang, Y., Hogrefe, C., and Xing, J.: Long-terms trends in sulfur and reactive nitrogen deposition across the Northern Hemisphere and United States, in: Air Pollution Modeling and Its Application XXVI, edited by: Mensink, C., Gong, W., and Hakami, A., ITM 2018, Springer Proceedings in Complexity, Springer, Cham, https://doi.org/10.1007/978-3-030-22055-6_7, 2020.

McCormick, M. P., Thomason, L. W., and Trepte, C. R.: Atmospheric effects of the Mt Pinatubo eruption, Nature, 373, 2, 1995.

Morrison, H., Thompson, G., and Tatarskii, V.: Impacts of cloud microphysics on the development of trailing stratiform precipitation in a simulated squall line: comparison of one- and two-moment schemes, Mon. Weather Rev. 137, 991–1007, 2009.

National Atmospheric Deposition Program's National Trends Network (NADP/NTN): Homepage, available at: http://nadp.slh.wisc.edu, last access: 30 July 2021.

National Centers for Environmental Prediction (NCEP): Final (FNL) Operational Global Analysis data, available at: https://rda.ucar.edu/datasets/ds083.2/, last access: 1 October 2020.

Pouliot, G., Denier van der Gon, H. A. C., Kuenen, J., Zhang, J., Moran, M. D., and Maker, P. A.: Analysis of the emission inventories and model-ready emission datasets of Europe and North America for phase 2 of the AQMEII project, Atmos. Environ., 115, 345–360, https://doi.org/10.1016/j.atmosenv.2014.10.061, 2015.

Sarwar, G., Gantt, B., Schwede, D., Foley, K., Mathur, R., and Saiz-Lopez, A.: Impact of enhanced ozone deposition and halogen chemistry on tropospheric ozone over the Northern Hemisphere, Environ. Sci. Technol., 49, 9203–9211, https://doi.org/10.1021/acs.est.5b01657, 2015.

Schmidt, A., Carslaw, K. S., Mann, G. W., Rap, A., Pringle, K. J., Spracklen, D. V., Wilson, M., and Forster, P. M.: Importance of tropospheric volcanic aerosol for indirect radiative forcing of climate, Atmos. Chem. Phys., 12, 7321–7339, https://doi.org/10.5194/acp-12-7321-2012, 2012.

Schmidt, A., Mills, M. J., Ghan, S., Gregory, J. M., Allan, R. P., Andrews, T., Bardeen, C. G., Conley, A., Forster, P. M., Gettelman, A., Portmann, R. W., Solomon, S., and Toon, O. B.: Volcanic radiative forcing from 1979 to 2015, J. Geophys. Res.-Atmos., 123, 12491–12508, https://doi.org/10.1002/2018JD028776, 2018.

Seinfeld, J. H. and Pandis, S. N.: Atmospheric Chemistry and Physics – From Air Pollution to Climate Change, 3rd ed., John Wiley & Sons, New York, 2016.

Simon, H. and Bhave, P. V.: Simulating the degree of oxidation in atmospheric organic particles, Environ. Sci. Technol., 46, 331–339, https://doi.org/10.1021/es202361w, 2012.

Smith, S. J., van Aardenne, J., Klimont, Z., Andres, R. J., Volke, A., and Delgado Arias, S.: Anthropogenic sulfur dioxide emissions: 1850–2005, Atmos. Chem. Phys., 11, 1101–1116, https://doi.org/10.5194/acp-11-1101-2011, 2011.

Smithsonian Institution: National Museum of Natural History, Global Volcanism Program, available at: https://volcano.si.edu, last access: 31 August 2020.

Tang, Y., Tong, D. Q., Yang, K., Lee, P., Baker, B., Crawford, A., Luke, W., Stein, A., Campbell, P. C., Ring, A., Flynn, J., Wang, Y., McQueen, J., Pan, L., Huang, J., and Stajner, I.: Air quality impacts of the 2018 Mt. Kilauea volcano eruption in Hawaii: A regional chemical transport model study with satellite-constrained emissions, Atmos. Environ., 227, 117648, https://doi.org/10.1016/j.atmosenv.2020.117648, 2020.

United States Environmental Protection Agency: CMAQ (Version 5.2), Zenodo [software], https://doi.org/10.5281/zenodo.1167892, 2017.

Warneck, P. and Williams, J.: The Atmospheric Chemist's Companion, Springer, New York, 2012.

Western Regional Air Partnership (WRAP): Homepage, available at: https://www.wrapair2.org/default.aspx, last access: 1 September 2020.

Wild, M.: Global dimming and brightening: A review, J. Geophys. Res.-Atmos., 114, D00D16, https://doi.org/10.1029/2008JD011470, 2009.

Xing, J., Mathur, R., Pleim, J., Hogrefe, C., Gan, C.-M., Wong, D. C., Wei, C., Gilliam, R., and Pouliot, G.: Observations and modeling of air quality trends over 1990–2010 across the Northern Hemisphere: China, the United States and Europe, Atmos. Chem. Phys., 15, 2723–2747, https://doi.org/10.5194/acp-15-2723-2015, 2015a.

Xing, J., Mathur, R., Pleim, J., Hogrefe, C., Gan, C.-M., Wong, D. C., Wei, C., and Wang, J.: Air pollution and climate response to aerosol direct radiative effects: A modeling study of decadal trends across the northern hemisphere, J. Geophys. Res.-Atmos., 120, 12221–12236, https://doi.org/10.1002/2015JD023933, 2015b.

Xing, J., Wang, J., Mathur, R., Pleim, J., Wang, S., Hogrefe, C., Gan, C. M., Wong, D. C., and Hao, J.: Unexpected benefits of reducing aerosol cooling effects, Environ. Sci. Technol., 50, 7527–7534, 2016.

Yamaji, K., Chatani, S., Yamaji, K., Itahashi, S., Saito, M., Takigawa, M., Morikawa, T., Kanda, I., Miya, Y., Komatsu, H., Sakurai, T., Morino, Y., Nagashima, T., Kitayama, K., Shimadera, H., Uranichi, K., Fujiwara, Y., Shintani, S., and Hayami, H.: Model inter-comparison for PM$_{2.5}$ components over urban areas in Japan in the J-STREAM framework, Atmosphere, 11, 222, https://doi.org/10.3390/atmos11030222, 2020.

Zhang, Q., Jimenez, J. L., Canagaratna, M. R., Allan, J. D., Coe, H., Ulbrich, I., Alfarra, M. R., Takami, A., Middlebrook, A. M., Sun, Y. L., Dzepina, K., Dunlea, E., Docherty, K., DeCarlo, P. F., Salcedo, D., Onasch, T., Jayne, J. T., Miyoshi, T., Shimono, A., Hatakeyama, S., Takegawa, N., Kondo, Y., Schneider, J., Drewnick, F., Borrmann, S., Weimer, S., Demerjian, K., Williams, P., Bower, K., Bahreini, R., Cottrell, L., Griffin, R. J., Rautiainen, J., Sun, J. Y., Zhang, Y. M., and Worsnop, D. R.: Ubiquity and dominance of oxygenated species in organic aerosols in anthropogenically-influenced Northern Hemisphere midlatitudes, Geophys. Res. Lett., 34, L13801, https://doi.org/10.1029/2007GL029979, 2007.

Zhang, Y., Liu, P., Pun, B., and Seigneur, C.: A Comprehensive Performance Evaluation of MM5-CMAQ for the Summer 1999 Southern Oxidants Study Episode, Part-I. Evaluation Protocols, Databases and Meteorological Predictions, Atmos. Environ., 40, 4825–4838, https://doi.org/10.1016/j.atmosenv.2005.12.043, 2006.

Zhang, Y., Vijayaraghavan, K., Wen, X.-Y., Snell, H. E., and Jacobson, M. Z.: Probing into regional ozone and particulate matter pollution in the United States: 1. A 1 year CMAQ simulation and evaluation using surface and satellite data, J. Geophys. Res., 114, D22304, https://doi.org/10.1029/2009JD011898, 2009.

Zhang, Y., Olsen, K. M., and Wang, K.: Fine scale modelling of agricultural air quality over the southeastern United States using two air quality models. Part I. Application and evaluation, Aerosol Air Qual. Res., 13, 1231–1252, https://doi.org/10.4209/aaqr.2012.12.0346, 2013.

Zhang, Y., Mathur, R., Bash, J. O., Hogrefe, C., Xing, J., and Roselle, S. J.: Long-term trends in total inorganic nitrogen and sulfur deposition in the US from 1990 to 2010, Atmos. Chem. Phys., 18, 9091–9106, https://doi.org/10.5194/acp-18-9091-2018, 2018.